

## SUPPLEMENTARY INFORMATION

### Nanoarchitected graphene/copper oxide nanoparticles/MoS<sub>2</sub> ternary thin films as highly efficient electrodes for aqueous sodium-ion battery

Maria K. Ramos<sup>a</sup>, Gustavo Martins<sup>a</sup>, Luiz H. Marcolino-Junior<sup>a</sup>, Márcio F. Bergamini<sup>a</sup>, Marcela M. Oliveira<sup>b</sup>, Aldo J. G. Zarbin<sup>a\*</sup>

<sup>a</sup>*Department of Chemistry, Federal University of Paraná (UFPR). CP 19032, 81531-980, Curitiba, PR, Brazil.*

<sup>b</sup>*Department of Chemistry and Biology, Technological Federal University of Paraná (UTFPR), Curitiba, PR, Brazil*

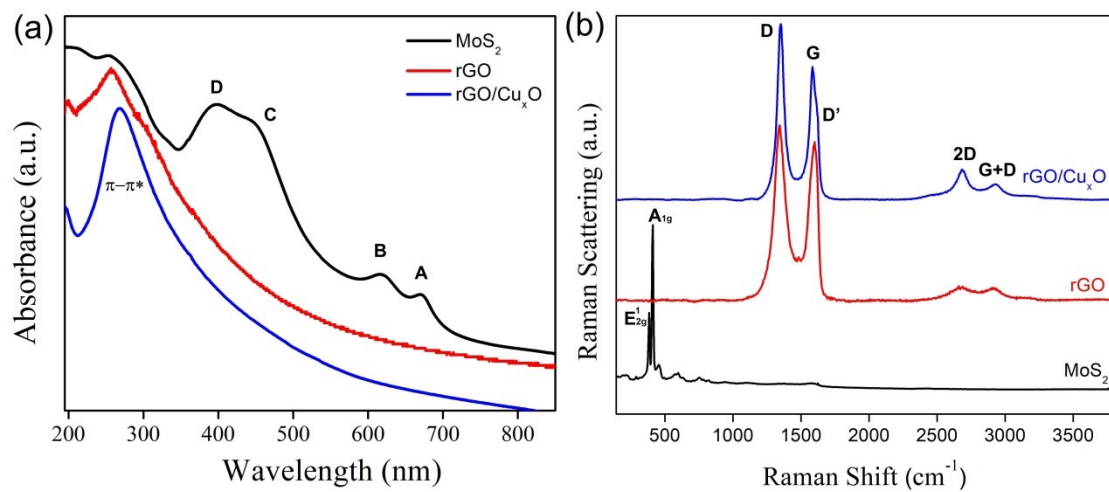


**Fig. S1:** UV-Vis (a) and Raman ( $\lambda = 532$  nm) (b) spectra of the control samples MoS<sub>2</sub> (black), rGO (red) and rGO/Cu<sub>x</sub>O (blue).

**Table S1:** The main bands observed by UV-Vis spectroscopy of the thin films deposited over planar quartz substrates.

Sample	Band A (nm)	Band B (nm)	Band C (nm)	Band D (nm)	Band $\pi-\pi^*$ (nm)
MoS <sub>2</sub>	673	621	453	392	-
rGO	-	-	-	-	259
rGO/Cu <sub>x</sub> O	-	-	-	-	270
rGO/MoS <sub>2</sub> -LbL	673	621	453	392	258
rGO/Cu <sub>x</sub> O/MoS <sub>2</sub> -LbL	673	621	453	392	264
rGO/MoS <sub>2</sub> -mixing	673	621	461	390	261
rGO/Cu <sub>x</sub> O/MoS <sub>2</sub> -mixing	673	621	462	390	267
rGO/MoS <sub>2</sub> -in situ	673	621	466	388	262
rGO/Cu <sub>x</sub> O/MoS <sub>2</sub> -in situ	673	621	477	389	269

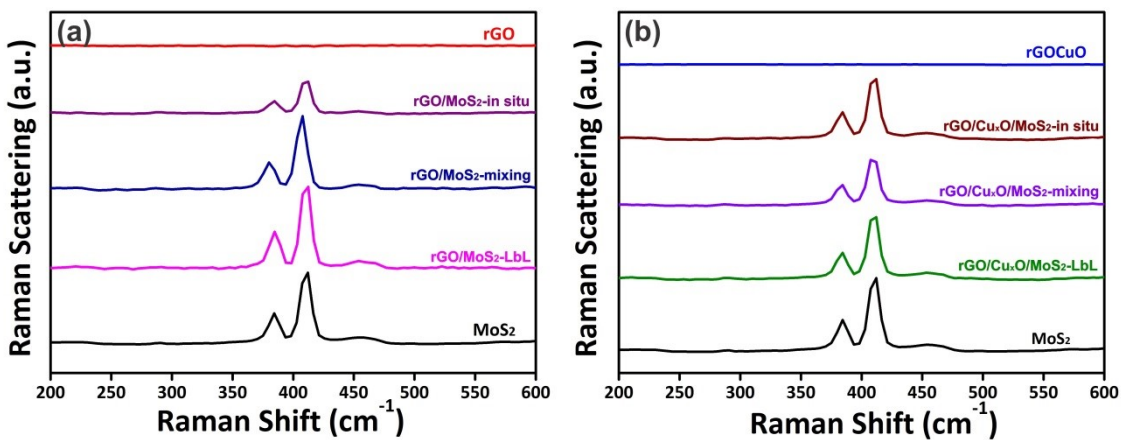


**Fig. S2:** Raman spectra ( $\lambda = 532$  nm) of the different nanocomposite set formed with rGO (a-b) and rGO/Cu<sub>x</sub>O (c-d).

**Table S2:** Raman bands and  $I_D/I_G$  ratio (calculated from the Lorentz deconvolution of the Raman spectra) observed in the thin film samples.

Sample	D Band (cm <sup>-1</sup> )	G Band (cm <sup>-1</sup> )	D' Band (cm <sup>-1</sup> )	MoS <sub>2</sub> A <sub>1g</sub> Band (cm <sup>-1</sup> )	MoS <sub>2</sub> E <sub>g</sub> Band (cm <sup>-1</sup> )	$I_D/I_G$
MoS <sub>2</sub>	-	-	-	412	384	-
rGO	1346	1591	-	-	-	$1.10 \pm 0.04$
rGO/Cu <sub>x</sub> O	1352	1588	1620	-	-	$1.58 \pm 0.10$
rGO/MoS <sub>2</sub> -LbL	1346	1591	-	412	384	$1.16 \pm 0.08$
rGO/Cu <sub>x</sub> O/MoS <sub>2</sub> -LbL	1351	1585	1618	411	384	$1.74 \pm 0.08$
rGO/MoS <sub>2</sub> -mixing	1342	1590	-	411	384	$1.17 \pm 0.14$
rGO/Cu <sub>x</sub> O/MoS <sub>2</sub> -mixing	1351	1589	1621	412	384	$1.88 \pm 0.22$
rGO/MoS <sub>2</sub> -in situ	1347	1592	-	411	385	$1.17 \pm 0.03$
rGO/Cu <sub>x</sub> O/MoS <sub>2</sub> -in situ	1352	1588	1616	412	384	$1.81 \pm 0.17$

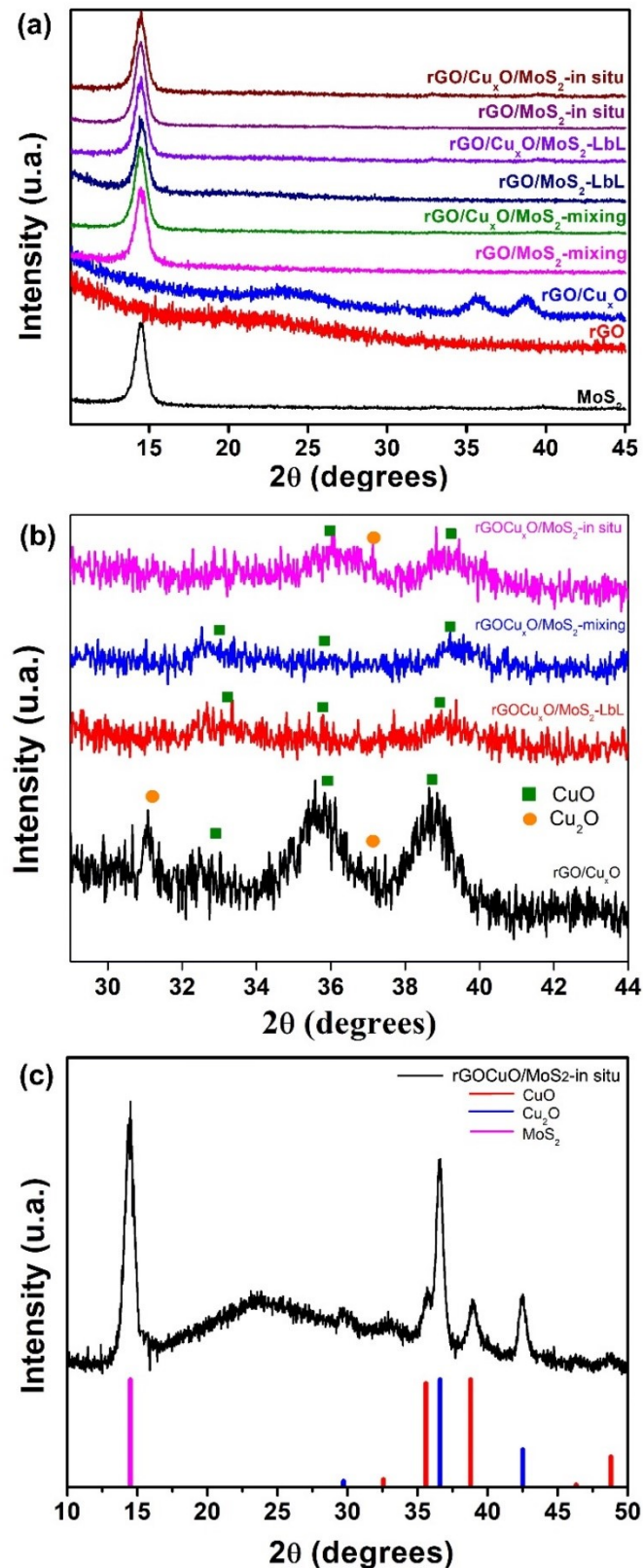


**Fig. S3:** X-ray diffraction patterns profile of thin films obtained using a low-angle mode thin film accessory (a-b); X-ray diffraction patterns profile of rGO/Cu<sub>x</sub>O/MoS<sub>2</sub>-in situ thin film obtained in a standard analysis. The colored traces in (c) corresponds to the peaks attributed to Cu<sub>2</sub>O (JCPDS 74-1230) and CuO (JCPDS 72-0629).

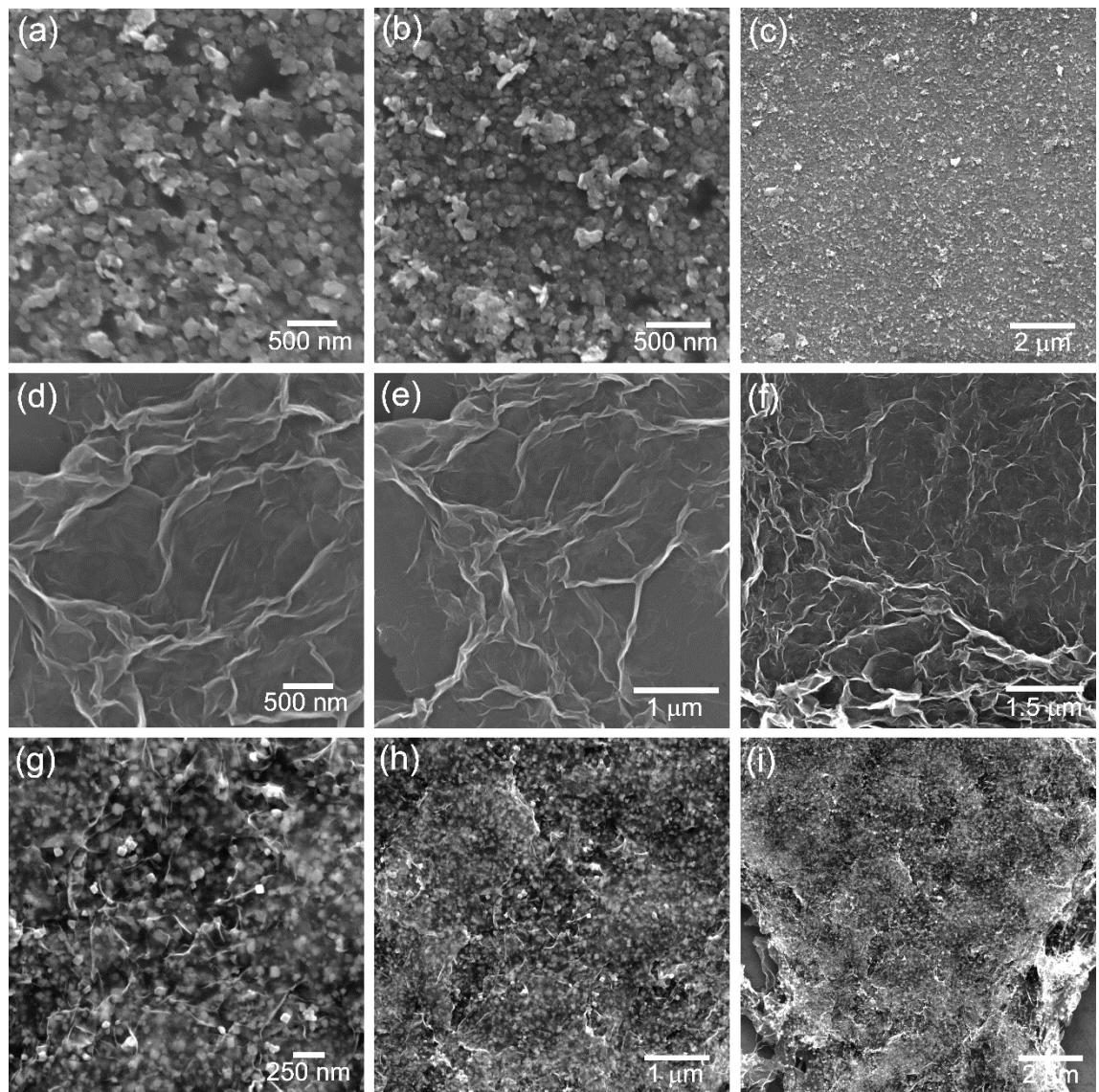


**Fig. S4:** SEM images of MoS<sub>2</sub> (a-c), rGO (d-f) and rGO/Cu<sub>x</sub>O (g-i) thin-films.

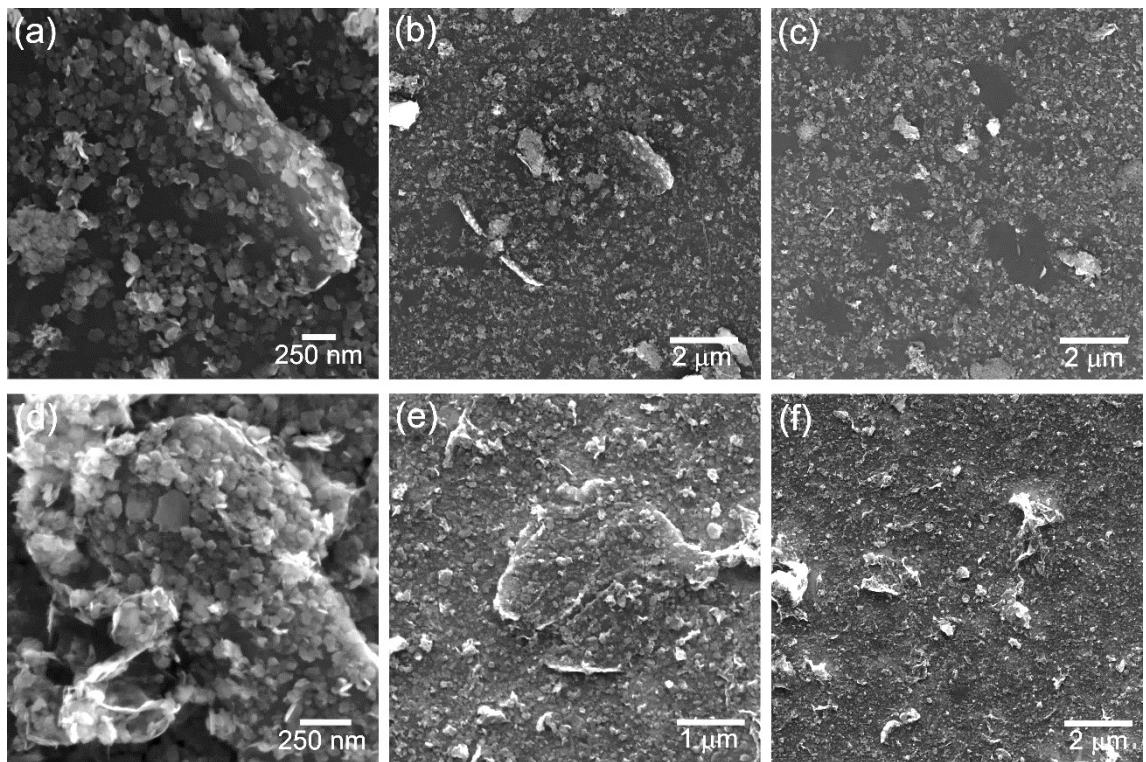


**Fig. S5:** SEM images of rGO/MoS<sub>2</sub>-LbL (a-c) and rGO/Cu<sub>x</sub>O/MoS<sub>2</sub>-LbL (d-f) thin-films.

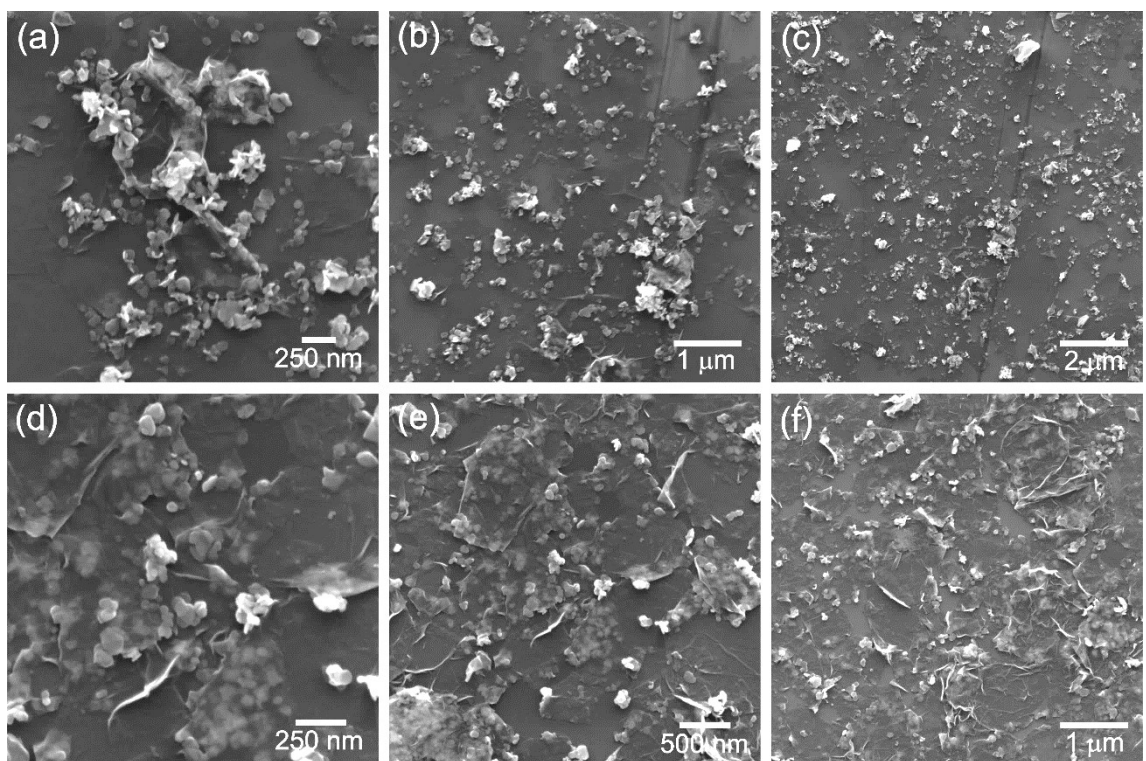


**Fig. S6:** SEM images of rGO/MoS<sub>2</sub>-mixing (a-c) and rGO/Cu<sub>x</sub>O/MoS<sub>2</sub>-mixing (d-f) thin-films.

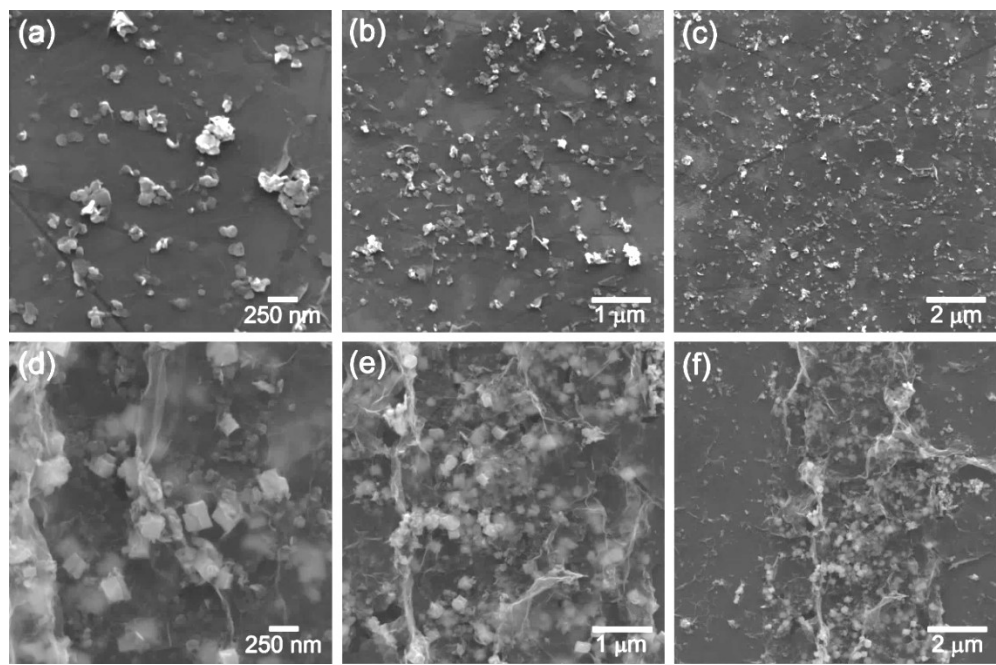


**Fig. S7:** SEM images of rGO/MoS<sub>2</sub>-in situ (a-c) and rGO/Cu<sub>x</sub>O/MoS<sub>2</sub>-in situ (d-f) thin-films.

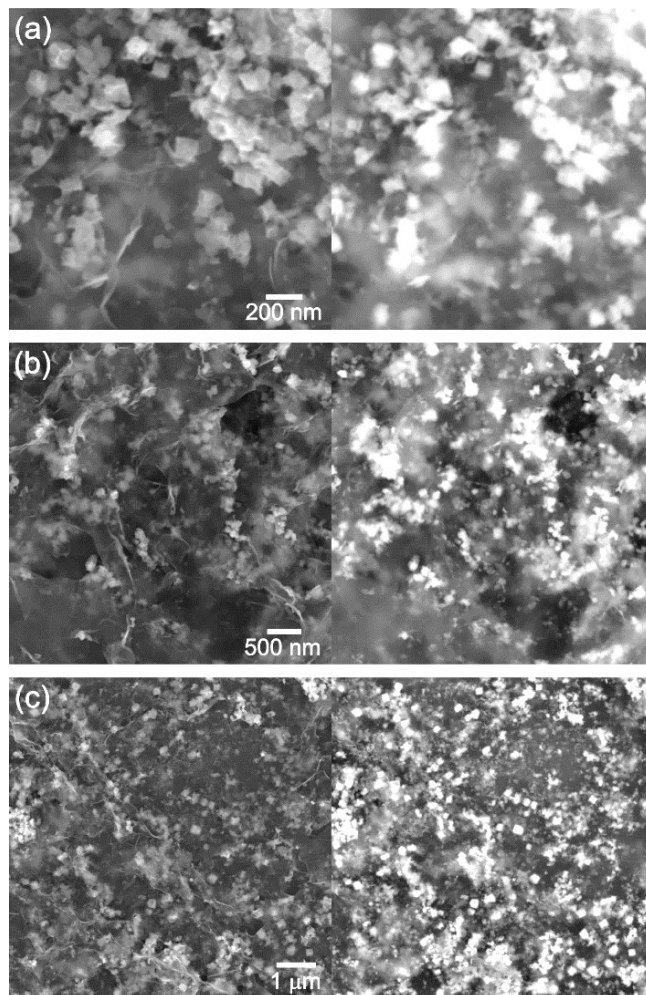


**Fig. S8:** SEM images of the rGO/Cu<sub>x</sub>O/MoS<sub>2</sub>-in situ sample, collected with secondary electron detector (left) and backscattered electrons (right).

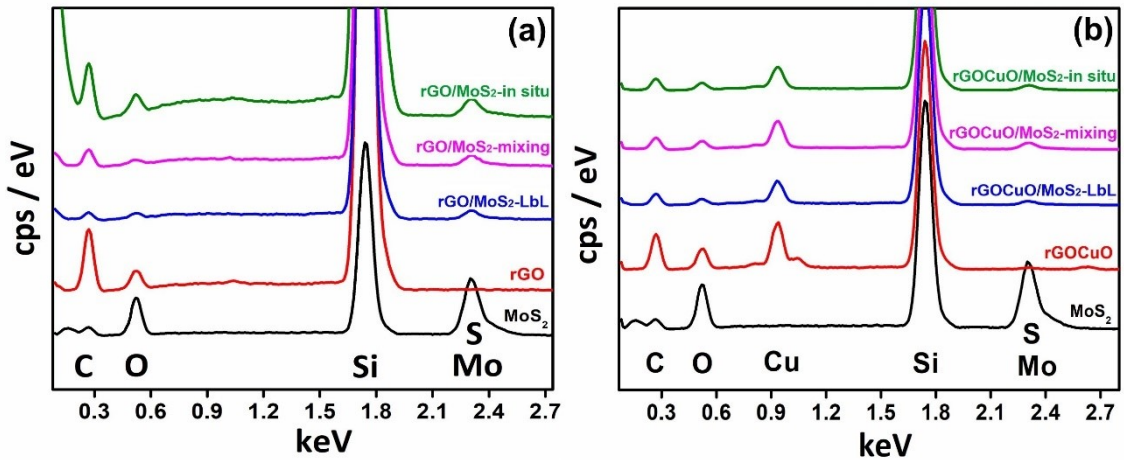


**Fig. S9:** Energy dispersive spectroscopy spectrums for rGO (a) and rGO/Cu<sub>x</sub>O (b) set.

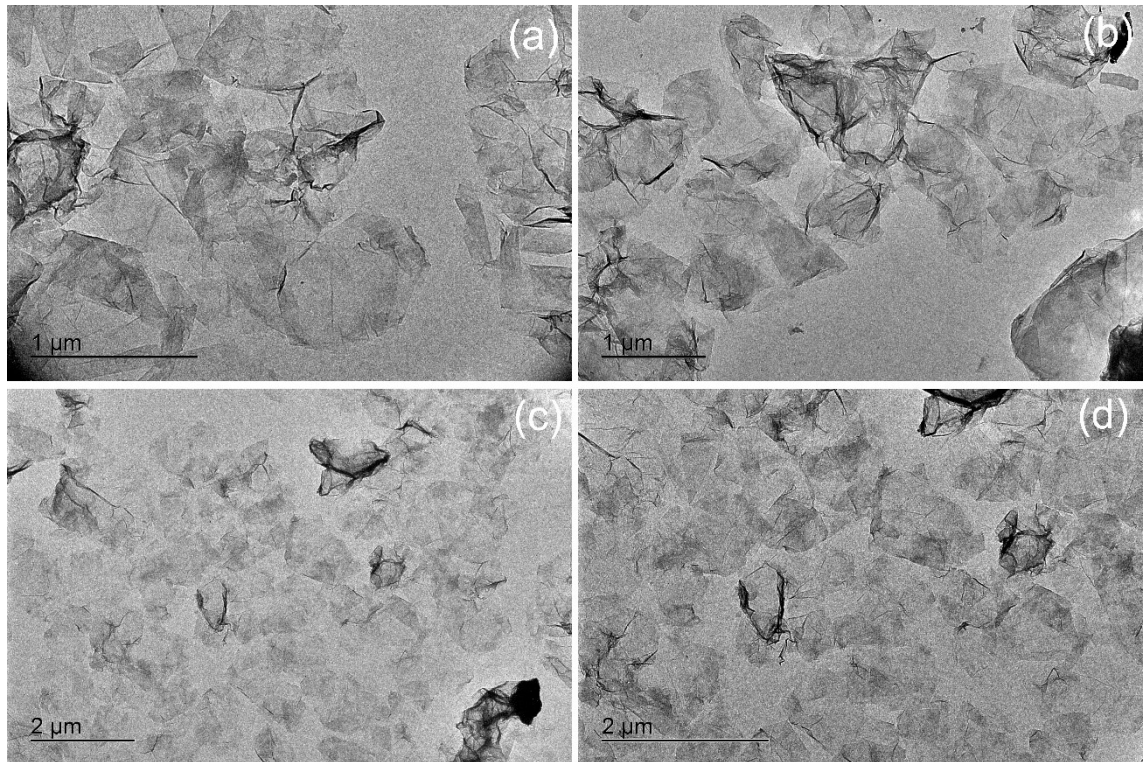


**Fig. S10:** Transmission microscopy and diffraction images of the rGO sample.

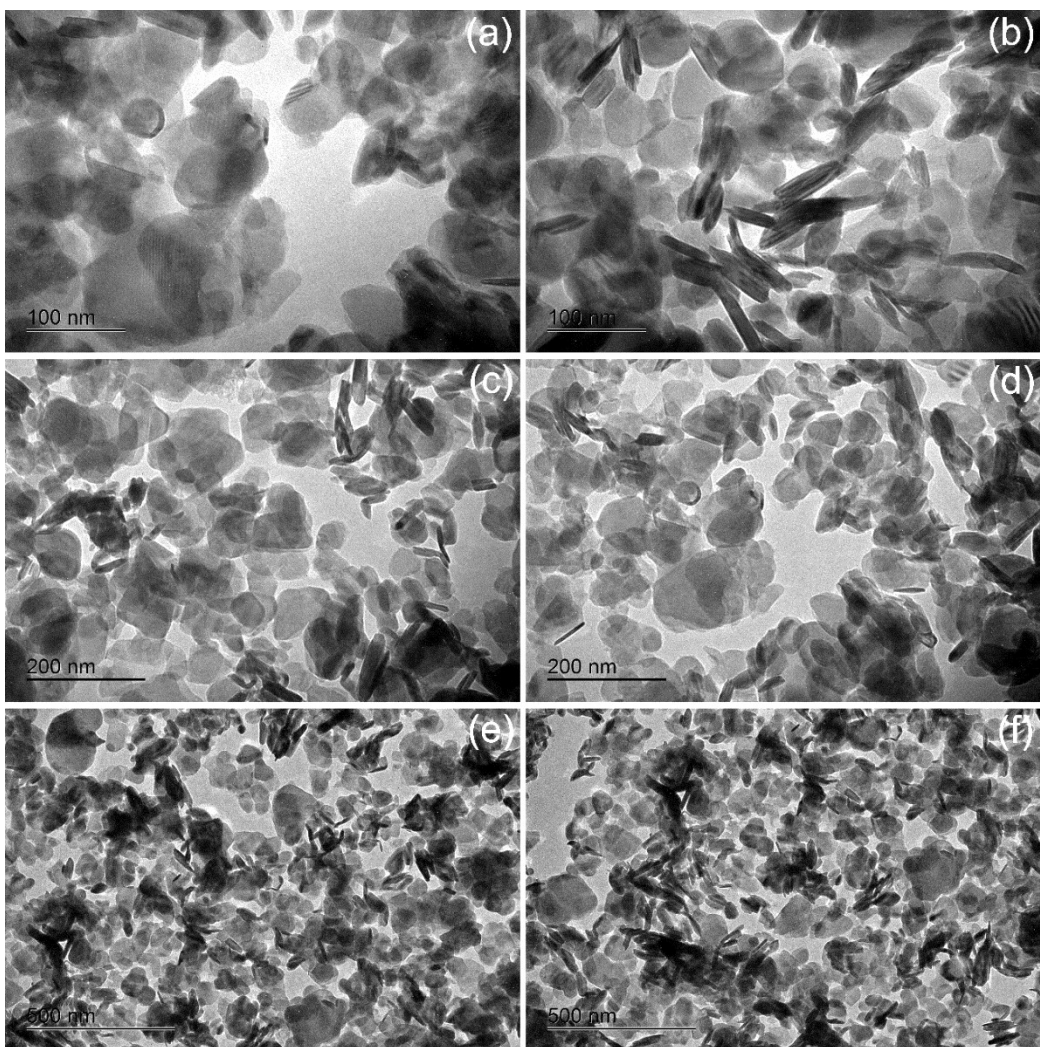


**Fig. S11:** Transmission microscopy images of the MoS<sub>2</sub> sample.

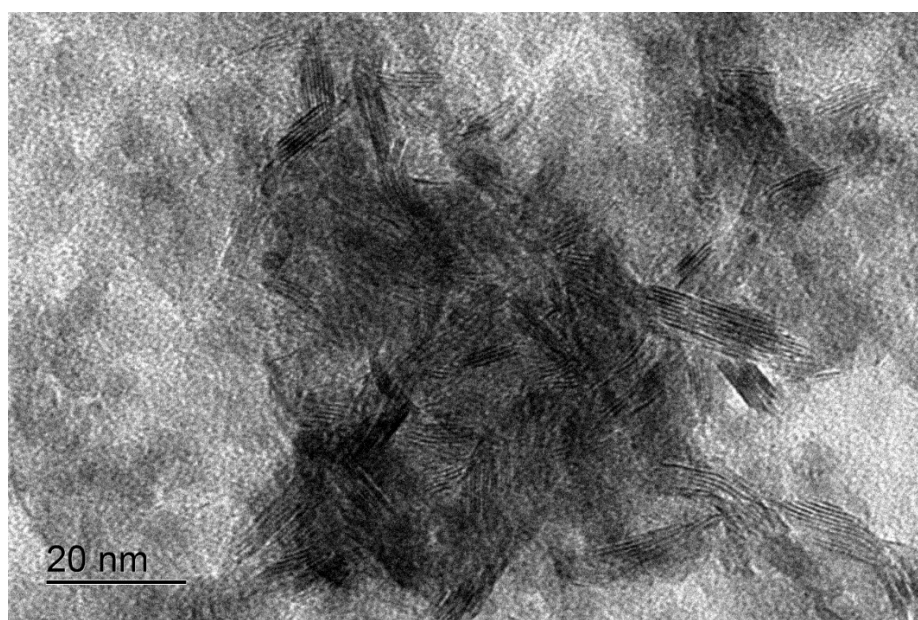


**Fig. S12:** Transmission microscopy image of MoS<sub>2</sub> sample.

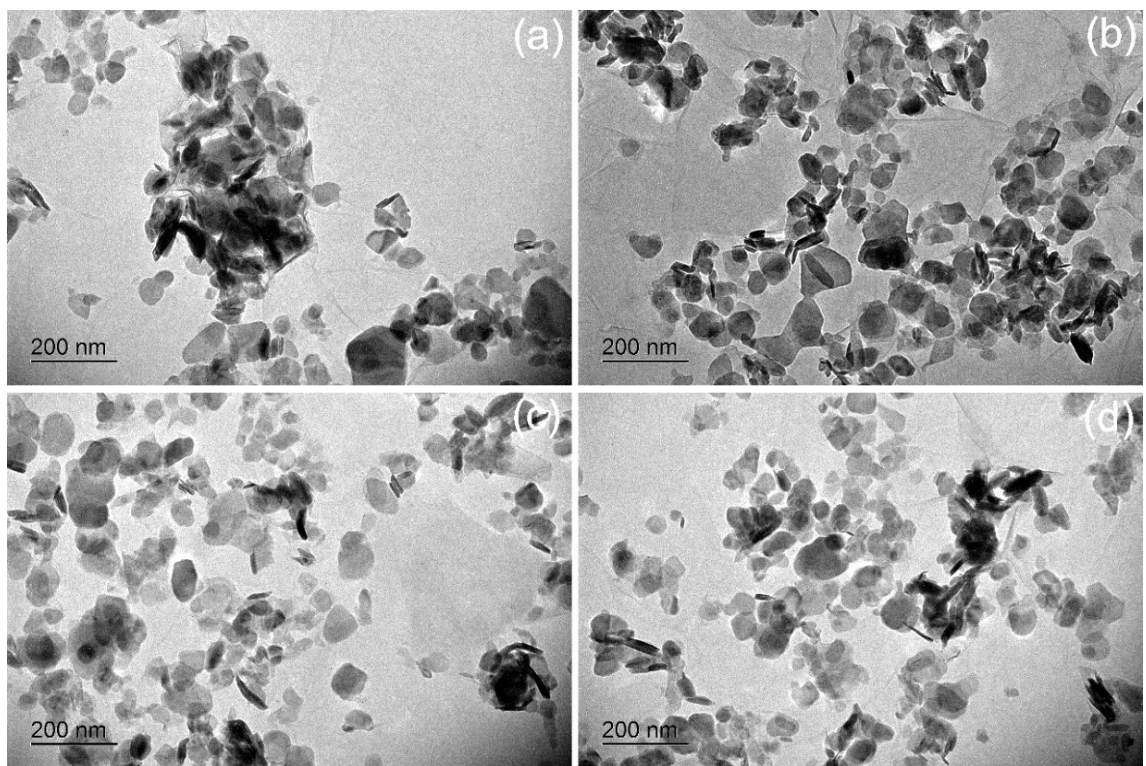


**Fig. S13:** Transmission microscopy images of the rGO/MoS<sub>2</sub> sample.

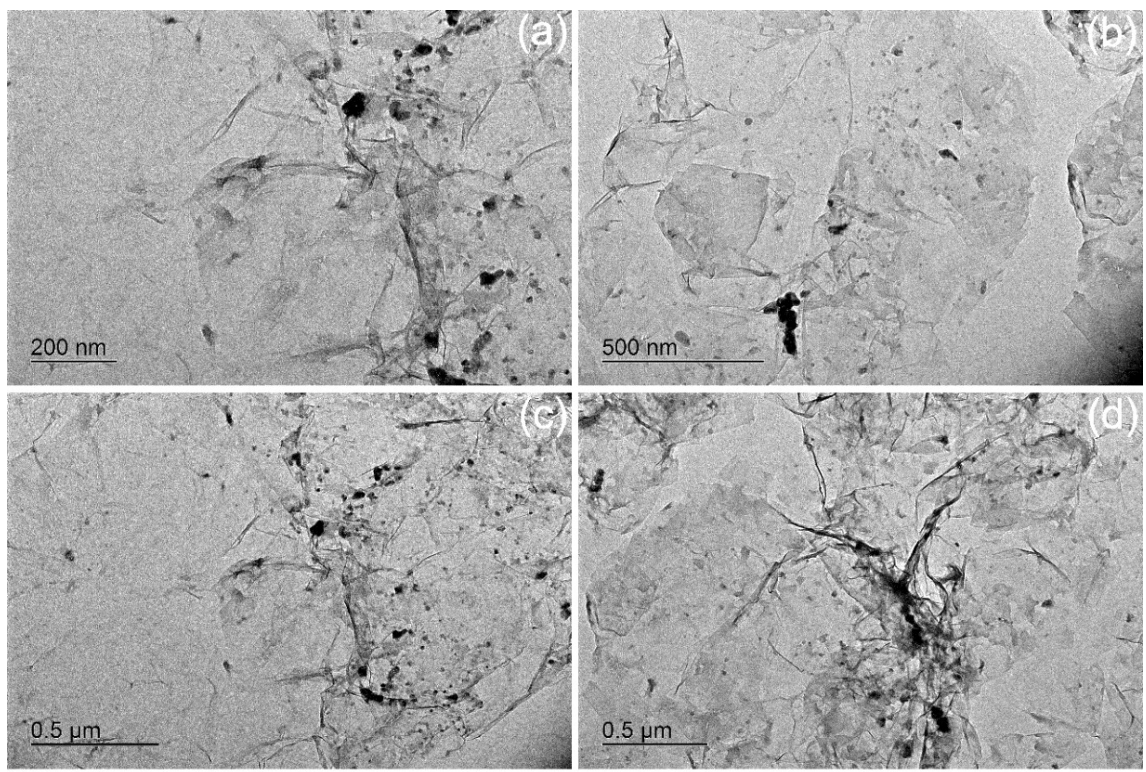


**Fig. S14:** Transmission microscopy images of the rGO/Cu<sub>x</sub>O sample.

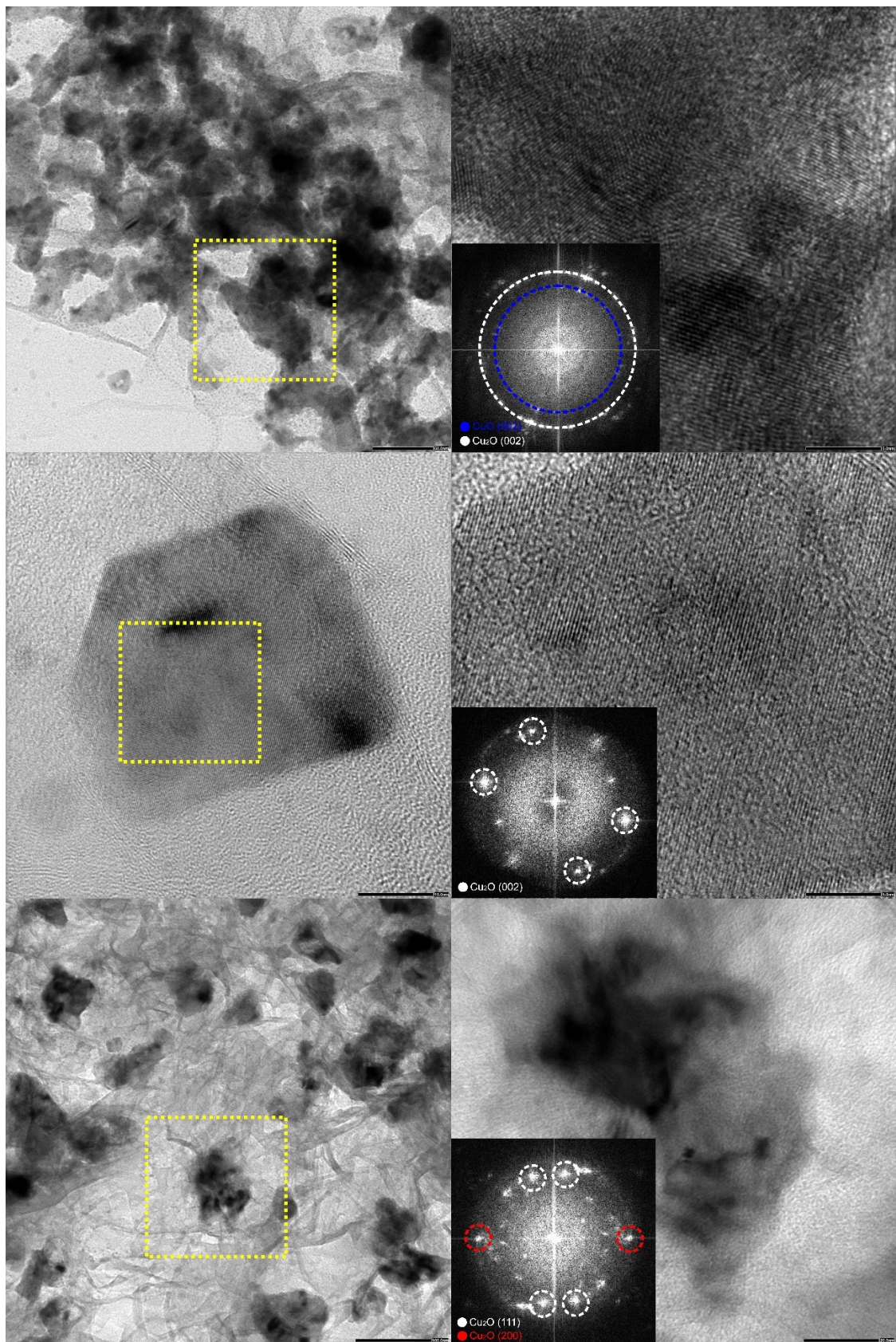


**Fig. S15:** High-resolution transmission electron microscopy (HRTEM) of rGO/Cu<sub>x</sub>O images and FFT analysis.

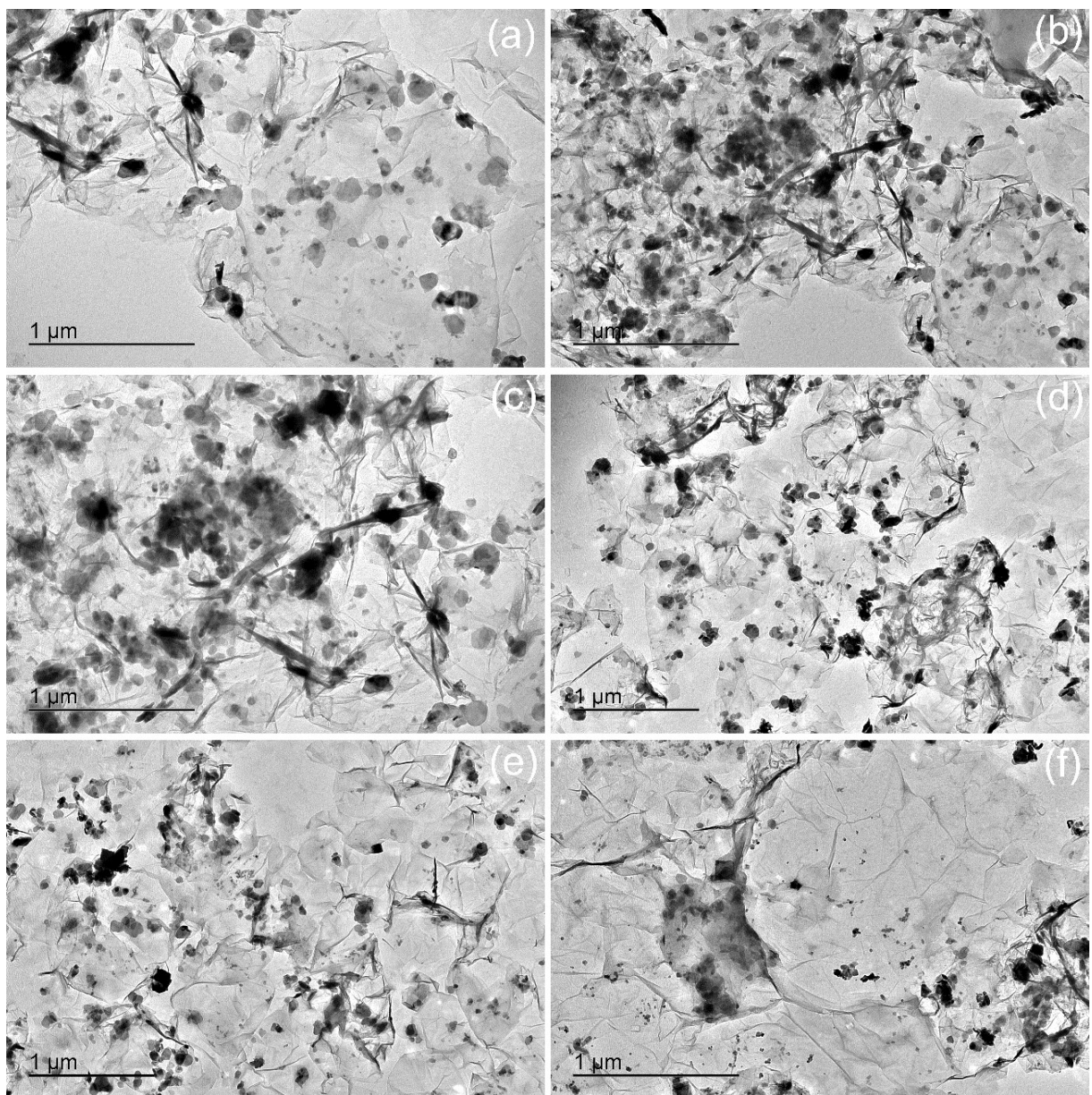


**Fig. S16:** Transmission electron microscopy images of the rGO/Cu<sub>x</sub>O/MoS<sub>2</sub>-in situ sample.

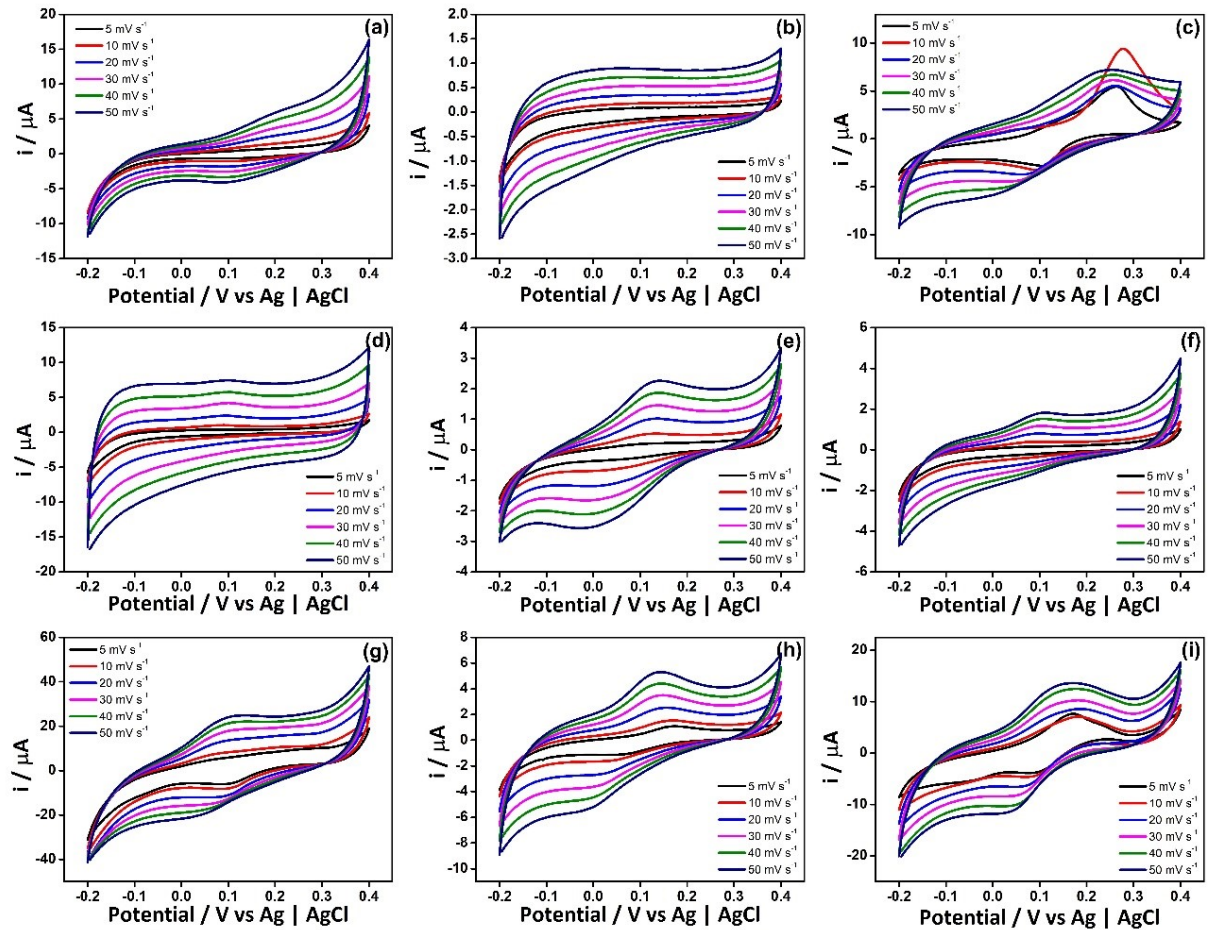


**Fig. S17:** Cyclic voltammograms at scan rates ranging from  $5 \text{ mV s}^{-1}$  to  $50 \text{ mV s}^{-1}$  of samples  $\text{MoS}_2$  (a); rGO (b); rGO/ $\text{Cu}_x\text{O}$  (c); rGO/ $\text{MoS}_2$ -LbL (d); rGO/ $\text{MoS}_2$ -mixing (e); rGO/ $\text{MoS}_2$ -in situ (f); rGO/ $\text{Cu}_x\text{O}/\text{MoS}_2$ -LbL (g); rGO/ $\text{Cu}_x\text{O}/\text{MoS}_2$ -mixing (h); and rGO/ $\text{Cu}_x\text{O}/\text{MoS}_2$ -in situ (i); obtained in the range of -0.2 to 0.4 V in  $0.1 \text{ mol L}^{-1} \text{ NaCl}$ .

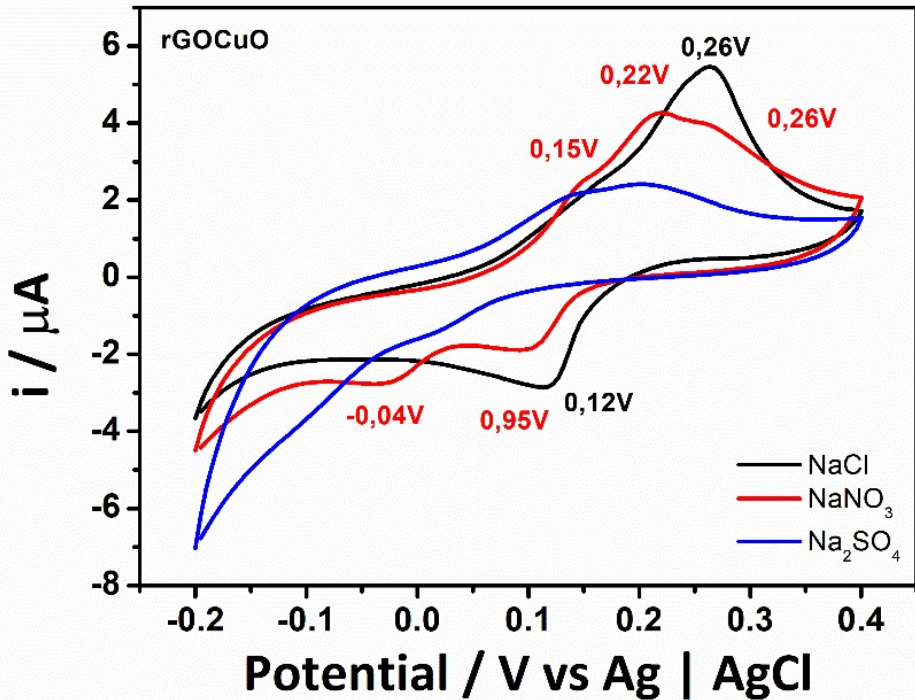


**Fig. S18:** Cyclic voltammetry profiles of rGO/Cu<sub>x</sub>O thin film in different electrolytes (aqueous solution, 0.1 mol L<sup>-1</sup>) at 5 mV s<sup>-1</sup> and -0.2 to 0.4 V range.

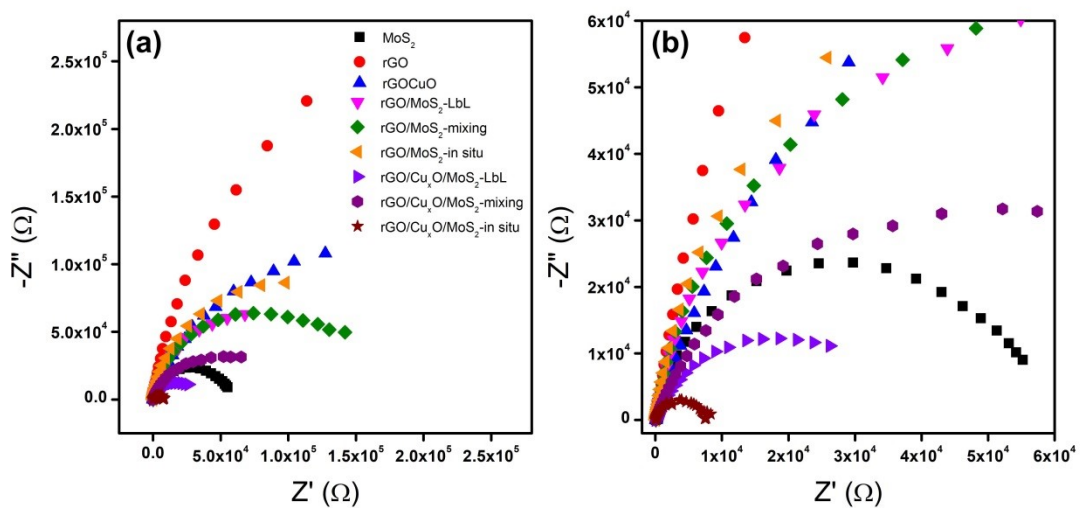


**Fig. S19:** Nyquist plot of the thin films. Electrolyte: aqueous solution of NaCl 0.1 mol L<sup>-1</sup> at -0.1 V.

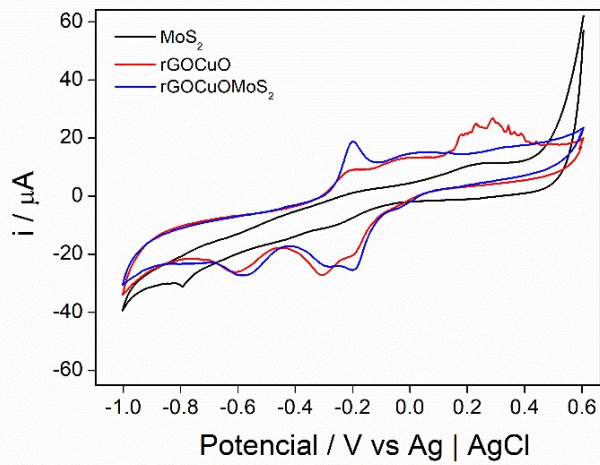


**Fig. S20:** Cyclic voltammetry of  $\text{MoS}_2$ , rGO/ $\text{Cu}_x\text{O}$  and rGO/ $\text{Cu}_x\text{O}/\text{MoS}_2$ -in situ films obtained in electrochemical quartz crystal microbalance. Films deposited over gold/quartz electrode, aqueous  $\text{NaCl}$  0.1 mol L<sup>-1</sup> solution as electrolyte.

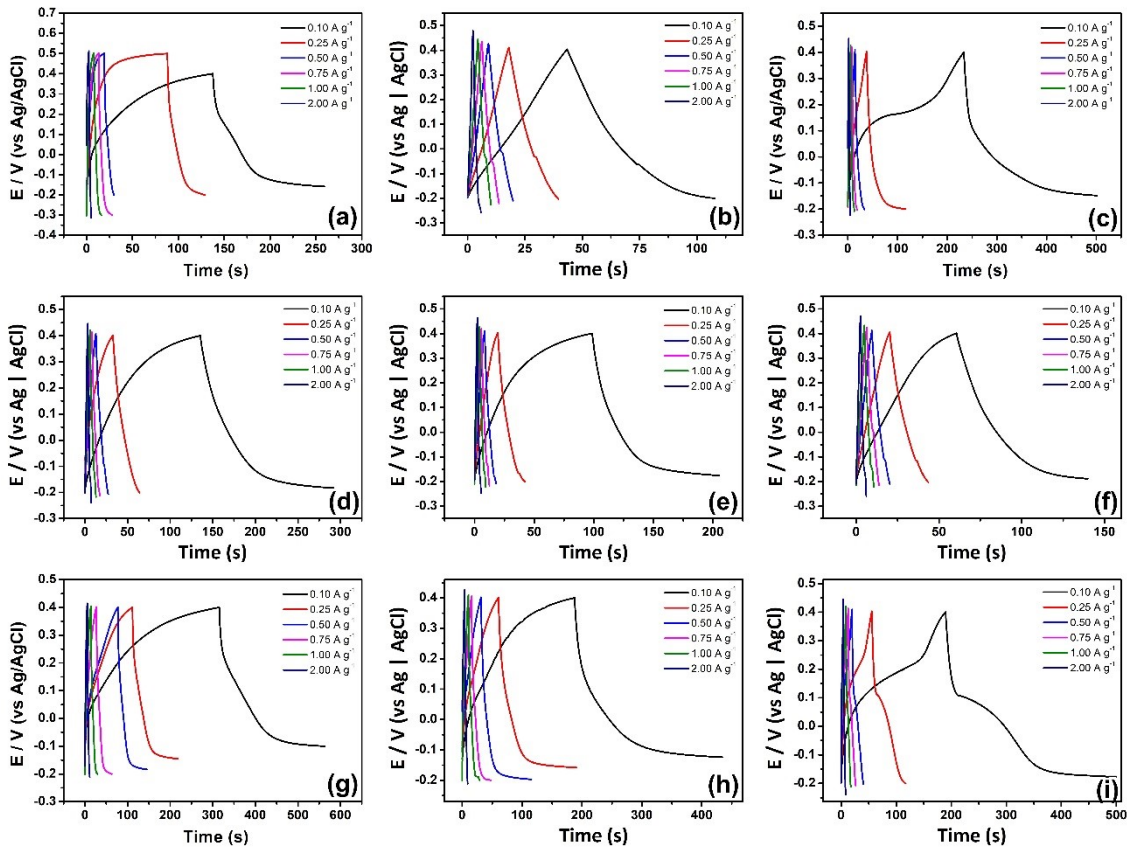


**Fig. S21:** Galvanostatic charge/discharge curves obtained at different currents (0.1, 0.25, 0.5, 0.75, 1 and 2 A g<sup>-1</sup>) of samples  $\text{MoS}_2$  (a); rGO (b); rGO/ $\text{Cu}_x\text{O}$  (c); rGO/MoS<sub>2</sub>-LbL (d); rGO/MoS<sub>2</sub>-mixing (e); rGOMoS<sub>2</sub>-in situ (f); rGO/Cu<sub>x</sub>O/MoS<sub>2</sub>-LbL (g); rGO/Cu<sub>x</sub>O/MoS<sub>2</sub>-mixing (h); and rGO/Cu<sub>x</sub>O/MoS<sub>2</sub>-in situ (i), obtained in the range from -0.2 to 0.4V in 0.1 mol L<sup>-1</sup> NaCl aqueous solution.

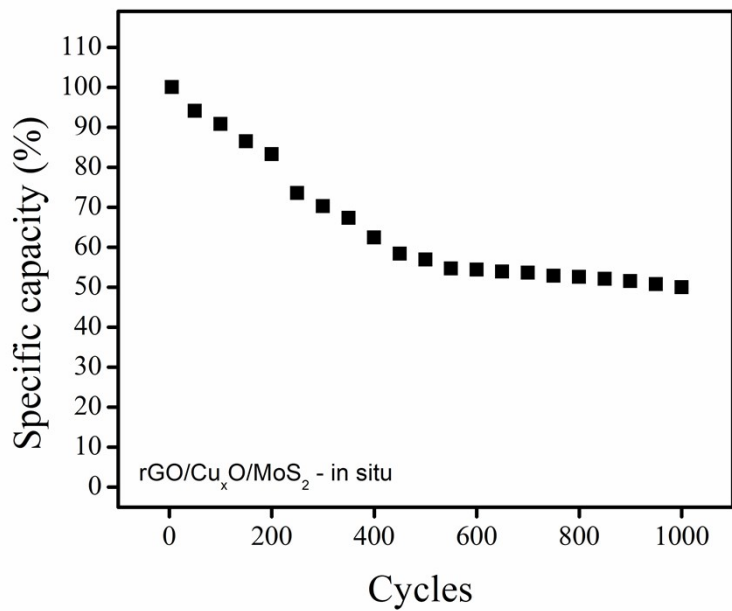


**Fig. S22:** Electrochemical stability after 1000 charge and discharge cycles (-0.2 to 0.4 V) of rGO/Cu<sub>x</sub>O/MoS<sub>2</sub>-in situ at 2A g<sup>-1</sup>, in 0.1 mol L<sup>-1</sup> NaCl aqueous solution.

**Table S3.** Values of capacity or specific capacitance of composites between MoS<sub>2</sub> and graphene, most used cations and electrolytes and retention rate found in the literature.

Samples	Electrode	Cation	Solvent	Current Density	Specific Capacity or Capacitance	Retention Rate	Reference
<b>rGO/Cu<sub>x</sub>O/MoS<sub>s</sub>-LbL</b>	Anode	Na <sup>+</sup>	Aqueous	100 mA g <sup>-1</sup>	1321 mA h g <sup>-1</sup>	78%	This work
<b>rGO/Cu<sub>x</sub>O/MoS<sub>2</sub>-mixing</b>	Anode	Na <sup>+</sup>	Aqueous	100 mA g <sup>-1</sup>	1056 mA h g <sup>-1</sup>	90%	This work
<b>rGO/Cu<sub>x</sub>O/MoS<sub>2</sub>-in situ</b>	Anode	Na <sup>+</sup>	Aqueous	100 mA g <sup>-1</sup>	1377 mA h g <sup>-1</sup>	100%	This work
<b>MoS<sub>2</sub>/G</b>	Anode	Li <sup>+</sup>	Organic	100 mA g <sup>-1</sup>	1902 mA h g <sup>-1</sup>	76.45%	3
<b>MoS<sub>2</sub>-SRGO</b>	Anode	Li <sup>+</sup>	Organic	50 mA g <sup>-1</sup>	896 mA h g <sup>-1</sup>	65%	4
<b>MoO<sub>2</sub>@MoS<sub>2</sub>/rGO</b>	Anode	Na <sup>+</sup>	Organic	100 mA g <sup>-1</sup>	604 mA h g <sup>-1</sup>	90.3%	5
<b>P-MoS<sub>2</sub>/PANI/rGO</b>	Anode	Li <sup>+</sup>	Aqueous	1 A g <sup>-1</sup>	431.7 F g <sup>-1</sup>	93.5%	6
<b>MoS<sub>2</sub>/rGO</b>	Anode	Li <sup>+</sup>	Organic	100 mA g <sup>-1</sup>	1289 mA h g <sup>-1</sup>	77%	7
<b>MoS<sub>2</sub>/G</b>	Anode	Li <sup>+</sup>	Organic	1 A g <sup>-1</sup>	1897 mA h g <sup>-1</sup>	91%	8
<b>mPF-MoS<sub>2</sub>@G</b>	Anode	Na <sup>+</sup>	Organic	100 mA g <sup>-1</sup>	488 mA h g <sup>-1</sup>	99.2%	9
<b>G/MoS<sub>2</sub></b>	Anode	Li <sup>+</sup>	Organic	100 mA g <sup>-1</sup>	1453 mA h g <sup>-1</sup>	-	10
<b>MoS<sub>2</sub>/PDC</b>	Anode	Li <sup>+</sup>	Organic	100 mA g <sup>-1</sup>	1354 mA h g <sup>-1</sup>	-	11
<b>MoS<sub>2</sub>/grafeno</b>	Anode	Li <sup>+</sup>	Organic	250 mA g <sup>-1</sup>	553 mA h g <sup>-1</sup>	99%	12
<b>v-MoS<sub>2</sub>/rGO</b>	Anode	Na <sup>+</sup>	Organic	2 A g <sup>-1</sup>	251 mA h g <sup>-1</sup>	95.7%	13
<b>MoS<sub>2</sub>/Gra</b>	Anode	Li <sup>+</sup>	Organic	100 mA g <sup>-1</sup>	1145 mA h g <sup>-1</sup>	88%	14
<b>MoS<sub>2</sub>/n-RGO</b>	Anode	Li <sup>+</sup>	Organic	100 mA g <sup>-1</sup>	1140 mA h g <sup>-1</sup>	94%	15
<b>MSRGO</b>	Anode	Na <sup>+</sup>	Organic	100 mA g <sup>-1</sup>	428 mA h g <sup>-1</sup>	90%	16
<b>CNTs/S@MoS<sub>2</sub>/G</b>	Cathode	Li <sup>+</sup>	Organic	0.1 C	1537 mA h g <sup>-1</sup>	78.3%	17
<b>MoS<sub>2</sub>/rGO</b>	Anode	Na <sup>+</sup>	Organic	100 mA g <sup>-1</sup>	338 mA h g <sup>-1</sup>	99%	18
<b>MoS<sub>2</sub>/GR</b>	Anode	Mg <sup>2+</sup>	Organic	20 mA g <sup>-1</sup>	210 mA h g <sup>-1</sup>	87%	19
<b>V-MoS<sub>2</sub>/rGOCTF</b>	Cathode	Li <sup>+</sup>	Organic	0.1 C	1379 mA h g <sup>-1</sup>	86%	20
<b>MoS<sub>2</sub>/grafeno</b>	Anode	Li <sup>+</sup>	Organic	100 mA g <sup>-1</sup>	1044 mA h g <sup>-1</sup>	-	21
<b>MoS<sub>2</sub>-G</b>	Anode	Na <sup>+</sup>	Organic	200 mA g <sup>-1</sup>	606 mA h g <sup>-1</sup>	100%	22
<b>N-GRs/MoS<sub>2</sub></b>	Anode	Li <sup>+</sup>	Organic	100 mA g <sup>-1</sup>	1151 mA h g <sup>-1</sup>	86%	23
<b>MoS<sub>2</sub>-RGO</b>	Anode	Li <sup>+</sup>	Organic	0.05 A g <sup>-1</sup>	1102 mA h g <sup>-1</sup>	74%	24
<b>PG-MoS<sub>2</sub></b>	Anode	Li <sup>+</sup>	Organic	100 mA g <sup>-1</sup>	1097 mA h g <sup>-1</sup>	-	25
<b>(MoS<sub>2</sub>)-grafeno</b>	Anode	Li <sup>+</sup>	Organic	100 mA g <sup>-1</sup>	1300 mA h g <sup>-1</sup>	93%	26
<b>(MoS<sub>2</sub>)-grafeno</b>	Anode	Na <sup>+</sup>	Organic	100 mA g <sup>-1</sup>	640 mA h g <sup>-1</sup>	93%	26
<b>MoS<sub>2</sub>-Gr</b>	Anode	Li <sup>+</sup>	Organic	0.1 C	1209 mA h g <sup>-1</sup>	100%	27
<b>FL-MoS<sub>2</sub>/grafeno</b>	Anode	Li <sup>+</sup>	Organic	100 mA g <sup>-1</sup>	980 mA h g <sup>-1</sup>	71.7%	28
<b>MoS<sub>2</sub>/RGO</b>	Anode	Li <sup>+</sup>	Organic	100 mA g <sup>-1</sup>	1180 mA h g <sup>-1</sup>	94%	29
<b>G/MoS<sub>2</sub></b>	Anode	KOH	Aqueous	0.6 mA g <sup>-1</sup>	48,58 F g <sup>-1</sup>	-	30
<b>MoS<sub>2</sub>/grafeno</b>	Cathode	Zn <sup>2+</sup>	Aqueous	0.05 A g <sup>-1</sup>	285 mA h g <sup>-1</sup>	88.2%	31
<b>MoS<sub>2</sub>/Gr/PAni</b>	Anode	Li <sup>+</sup>	Organic	200 mA g <sup>-1</sup>	785 mA h g <sup>-1</sup>	82.3%	32
<b>MoO<sub>2</sub>@MoS<sub>2</sub>/rGO</b>	Anode	Li <sup>+</sup>	Organic	100 mA g <sup>-1</sup>	604 mA h g <sup>-1</sup>	90.3%	5
<b>CNTs/S@MoS<sub>2</sub>/Gr</b>	Cathode	Li <sup>+</sup>	Organic	0.1 C	1537 mA h g <sup>-1</sup>	78.3%	17
<b>MS/MO/CNT/G</b>	Anode	Li <sup>+</sup>	Organic	100 mA g <sup>-1</sup>	640 mA h g <sup>-1</sup>	78.5%	33
<b>PEDOT/MoS<sub>2</sub>/Gr</b>	Anode	Li <sup>+</sup>	Organic	-	1143.7 F g <sup>-1</sup>	73.3%	34
<b>CuO/MoS<sub>2</sub>/rGO</b>	Anode	Li <sup>+</sup>	Organic	1 A g <sup>-1</sup>	1445 F g <sup>-1</sup>	91%	35

## References

- 1 W. S. Hummers and R. E. Offeman, *J. Am. Chem. Soc.*, 1958, **80**, 1339.
- 2 H. Mehl, C. F. Matos, E. G. C. Neiva, S. H. Domingues and A. J. G. Zarbin, *Quim. Nova*, 2014, **37**, 1639–1645.
- 3 J. Wang, X. Zhao, Y. Fu and X. Wang, *Appl. Surf. Sci.*, 2017, **399**, 237–244.
- 4 M. Choi, S. K. Koppala, D. Yoon, J. Hwang, S. M. Kim and J. Kim, *J. Power Sources*, 2016, **309**, 202–211.
- 5 Y. Luo, X. Ding, X. Ma, D. Liu, H. Fu and X. Xiong, *Electrochim. Acta*, 2021, **388**, 138612.
- 6 J. Chao, L. Yang, H. Zhang, J. Liu, R. Hu and M. Zhu, *J. Power Sources*, 2020, **450**, 227680.
- 7 Z. Yu, J. Ye, W. Chen, S. Xu and F. Huang, *Carbon N. Y.*, 2017, **114**, 125–133.
- 8 M. Yang, S. Ko, J. S. Im and B. G. Choi, *J. Power Sources*, 2015, **288**, 76–81.
- 9 J. Deng, C. Zeng, C. Ma, J. Fold von Bülow, L. Zhang, D. Deng, Z. Tian and X. Bao, *Mater. Today Energy*, 2018, **8**, 151–156.
- 10 T. Wang, G. Zhao, C. Sun, L. Zhang, Y. Wu, X. Hao and Y. Shao, *Adv. Mater. Interfaces*, 2017, **4**, 1–8.
- 11 Y. Huang, J. Zou, L. Luo, Z. Zhao, H. Liu, Y. Huang, A. Ren and Z. Wang, *J. Mater. Sci.*, 2022, **57**, 1246–1260.
- 12 S. Mateti, M. M. Rahman, P. Cizek and Y. Chen, *RSC Adv.*, 2020, **10**, 12754–12758.
- 13 H. Li, X. Wen, F. Shao, S. Xu, C. Zhou, Y. Zhang, H. Wei and N. Hu, *J. Alloys Compd.*, 2021, **877**, 160280.
- 14 Y. Liu, X. He, D. Hanlon, A. Harvey, J. N. Coleman and Y. Li, *ACS Nano*, 2016, **10**, 8821–8828.
- 15 N. Lingappan and D. J. Kang, *Electrochim. Acta*, 2016, **193**, 128–136.
- 16 J. Li, H. Tao, Y. Zhang and X. Yang, *J. Electrochem. Soc.*, 2019, **166**, A3685–A3692.
- 17 X. Fang and M. Zhang, *Ionics (Kiel)*., 2021, **27**, 3875–3885.
- 18 L. David, R. Bhandavat and G. Singh, *ACS Nano*, 2014, **8**, 1759–1770.
- 19 C. Wu, G. Zhao, X. Yu, C. Liu, P. Lyu, G. Maurin, S. Le, K. Sun and N. Zhang, *Chem. Eng. J.*, 2021, **412**, 128736.
- 20 B. Cui, X. Cai, W. Wang, P. Saha and G. Wang, *J. Energy Chem.*, 2022, **66**, 91–99.
- 21 V. O. Koroteev, S. G. Stolyarova, A. A. Kotsun, E. Modin, A. A. Makarova, Y. V. Shubin, P. E. Plyusnin, A. V. Okotrub and L. G. Bulusheva, *Carbon N. Y.*, 2021, **173**, 194–204.

- 22 S. Anwer, Y. Huang, B. Li, B. Govindan, K. Liao, W. J. Cantwell, F. Wu, R. Chen and L. Zheng, *ACS Appl. Mater. Interfaces*, 2019, **11**, 22323–22331.
- 23 Z. Xiao, L. Sheng, L. Jiang, Y. Zhao, M. Jiang, X. Zhang, M. Zhang, J. Shi, Y. Lin and Z. Fan, *Chem. Eng. J.*, 2021, **408**, 127269.
- 24 M. Choi, J. Hwang, H. Setiadi, W. Chang and J. Kim, *J. Supercrit. Fluids*, 2017, **127**, 81–89.
- 25 W. Qiu, J. Jiao, J. Xia, H. Zhong and L. Chen, *RSC Adv.*, 2014, **4**, 50529–50535.
- 26 S. Kalluri, K. H. Seng, Z. Guo, A. Du, K. Konstantinov, H. K. Liu and S. X. Dou, *Sci. Rep.*, 2015, **5**, 1–8.
- 27 J. Han, H. Jang, H. Thi Bui, M. Jahn, D. Ahn, K. Cho, B. Jun, S. U. Lee, S. Sabine, M. Stöger-Pollach, K. Whitmore, M. M. Sung, V. Kutwade, R. Sharma and S. H. Han, *J. Alloys Compd.*, 2021, **862**, 158031.
- 28 L. Xu, Z. Jiao, P. Hu, Y. Wang, Y. Wang and H. Zhang, *ChemElectroChem*, 2016, **3**, 1503–1512.
- 29 G. Liu, Y. Feng, Y. Li, M. Qin, H. An, W. Hu and W. Feng, *Part. Part. Syst. Charact.*, 2015, **32**, 489–497.
- 30 R. N. A. R. Seman and M. A. Azam, *J. Sci. Adv. Mater. Devices*, 2020, **5**, 554–559.
- 31 S. Li, Y. Liu, X. Zhao, Q. Shen, W. Zhao, Q. Tan, N. Zhang, P. Li, L. Jiao and X. Qu, *Adv. Mater.*, 2021, **33**, 1–9.
- 32 S. Han, Y. Ai, Y. Tang, J. Jiang and D. Wu, *RSC Adv.*, 2015, **5**, 96660–96664.
- 33 J. Li, S. Du, H. Tao and X. Yang, *Ionics (Kiel)*, 2021, **27**, 75–84.
- 34 D. Sarmah and A. Kumar, *J. Energy Storage*, 2021, **35**, 102289.
- 35 P. S. Selvamani, J. J. Vijaya, L. J. Kennedy, B. Saravanakumar, M. Bououdina and J. R. Rajabathar, *Synth. Met.*, 2021, **278**, 116843.